NORWEGIAN JOURNAL OF GEOLOGY
https://dx.doi.org/10.17850/njg102-3-04

GEOLOGICAL SOCIETY OF NORWAY

Extreme precipitation induced landslide event on 30 July 2019 in Jølster, western Norway

Denise Christina Rüther[1], Heidi Hefre[2] & Lena Rubensdotter[3, 4]

[1]HVL, Department of Environmental Sciences, Røyrgata 6, N-6856 Sogndal.
[2]NGI, Norwegian Geotechnical Institute, Sandakerveien 140, N-0484 Oslo.
[3]NGU, Geohazards and Earth Observation, Leiv Eirikssons vei 39, N-7040 Trondheim.
[4]UNIS, Department of Arctic Geology, P.O. Box 156. N-9171 Longyearbyen.

E-mail corresponding author (Denise Christina Rüther): denise.christina.ruther@hvl.no

Keywords:
- *Torrential rain induced shallow landslides*
- *Torrential rain on dry ground*
- *Debris flows*
- *Trigger mechanism*
- *Landslide characteristics*

Received:
10. May 2022

Accepted:
26. September 2022

Published online:
18. October 2022

A torrential rain event struck western Norway on Tuesday 30 July 2019. Most severely affected was the Jølster community, where numerous landslides and floods damaged public infrastructure and private property. This resulted in one fatality, 150 people evacuated from the area and the closure of Highway E39, the main coastal transport route in Norway. Weather radar data reveal large spatial and temporal variations in rainfall intensity and areas with highest intensities correspond to observed shallow landslide clusters where the 200-year rainfall event magnitude was clearly exceeded. The majority of 120 shallow landslide source areas share common characteristics: they are situated above or at the tree line, in thin to very thin soil, in contact with the bedrock or large boulders and in rather steep terrain (>30 degrees). Several lines of evidence suggest that soil in the source areas was not fully saturated, but instead failed due to locally high porewater pressures as short and intense rainfall on dry ground led to water infiltration through open cracks in the surface cover, and commonly at soil-bedrock or soil-boulder contacts. The most far-reaching debris flows of the event have steep upper transport areas, in places with cliff sections, which created sufficient flow-momentum despite small starting volumes. We note that erosion along the flow path was relatively superficial since incomplete soil saturation with depth likely prevented deeper entrainment. Consequently, water-to-solid ratios in the mobilised material was high and the runout possibly longer but less destructive compared to more deep-seated landslide events. This type of summer torrential rain on unsaturated soil require adjustments to how Norwegian society predicts and prepares for shallow landslides triggered during these events, compared with landslides following longer-lasting rainfall.

Rüther, D. C., Hefre, H. & Rubensdotter, L. 2022: Extreme precipitation induced landslide event on 30 July 2019 in Jølster, western Norway. *Norwegian Journal of Geology 102*, 202212.
https://dx.doi.org/10.17850/njg102-3-4

Glossary of mass movements

In this study, we distinguish several types of shallow landslides based primarily on movement type and included material, following Varnes (1978) and Hungr et al. (2014). Acknowledging that different landslide terms are often used interchangeably, we here clarify the terminology for shallow landslides used in this study.

Firstly, we distinguish shallow landslides and debris flows from **debris floods**. Debris floods are channelised flows in which most of the sediment is transported particle-by-particle as bedload in the fluvial stream. Sediment entrainment occurs without point release through continued riverbed and riverbank erosion. During the Jølster event, debris floods were observed in small meadow streams as well as in large torrents.

Shallow landslides have a defined source area and can be characterised as point release.

When the debris moves translationally as a coherent body over a sliding plane, we refer to the shallow landslide as a **debris slide**. In the field, the sliding planes can be identified by a compact surface of soft sediment or bedrock exposure, sometimes with striations. We observe that a debris slide initiation develops into a debris flow where a critical mass and/or critical slope angle needed to develop into a debris flow is attained.

In this study, we also see examples of rotational sliding or **slumping** as thin grass-bound topsoil overturns under the load of water saturation. Like the debris slides, these have generally short runouts. However, unlike deeper-seated slumps in clay-rich soil where cohesion prevents translation into debris flows, overturned thin topsoils may develop into a debris flow in cases where a critical mass and/or critical slope angle is attained.

Shallow landslides with a flow behaviour, where the material moves more as a fluid downslope, are referred to as **debris flows** (when channelised) or **debris avalanches** (when non-channelised). Debris flows and avalanches exhibit a turbulent internal movement in the flow, causing friction between solid particles and typically involve deposition of levees along the mid- and lower flow path.

Slush flows are a form of very wet snow avalanches formed by water-logged snow which collapses under its own weight when the water content becomes too great. Whilst not classified under the category of shallow landslides, slush flows often erode and incorporate debris along the path and may therefore transition into low viscosity debris flows when approaching the valley bottoms. They can hence become classified as debris flows in event registration, which is often made observing the runout, rather than the initiation. Slush flows did not occur at the 2019 Jølster event but are found to be a common mass movement type in the studied area.

Introduction

In Norway, shallow landslides are predominantly triggered by long-lasting and/or intense rainfall, commonly in combination with snowmelt (e.g., Jaedicke et al., 2008). It is well established that porewater pressure is crucial in triggering shallow debris flows and slides (Johnson & Sitar, 1990; Iverson, 1997; Bogaard & Greco, 2016). Therefore, rainfall-induced landslides in Norway typically occur in the autumn and spring when porewater pressures are generally high due to sustained rainfall and/or snowmelt (e.g., Bondevik & Sorteberg, 2021). While high porewater pressure is generally acknowledged

as a landslide trigger, few studies have yet focused on the effect of drought and low porewater pressure prior to intense rainfall, in particular in the northern temperate zone. Tichavský et al. (2019) showed that for Central Europe low groundwater level, drought, the opening of tension cracks and weakening of soil anchorage facilitate failure upon rainfall. In threshold studies, it is well established that the minimum average rainfall intensity required to trigger shallow landslides increases linearly for rainfall events of shorter duration (with durations ranging from 35 days to 10 min; Guzzetti et al., 2008).

Public and professional awareness of floods and landslides triggered by summer torrential rains in Norway has in the past years been raised due to devastating events in urban as well as rural environments. In western Norway, the most prominent events caused by convective rainstorms were Blakset (Stryn municipality) on 25 July 2011, Utvik (Stryn municipality) on 24 July 2017 and undeniably the most destructive at Vassenden (former Jølster municipality, merged to Sunnfjord municipality in January 2020) on 30 July 2019, which is the focus of this study. In response to the Blakset and Utvik events, the Norwegian Meteorological Institute (MET) and Norwegian Water and Energy Directorate (NVE) are working to improve their methodology for weather and landslide forecasting and warning services. MET and NVE also cooperate closely in issuing a newly established category of heavy rainfall warnings. The improvement of methodologies for predicting and handling these events is of particular importance since heavy summer rainstorms of this dimension are expected to become more frequent in a warming climate (Hanssen-Bauer et al., 2009).

The mapping of 30 July 2019 landslides shown in Figs. 1A, B & 2A is based on 10 m resolution Normalized Difference Vegetation Index (NDVI) images from Sentinel-2 satellite data mapped by Lindsay et al. (2022) who identified 120 cases of shallow landslides (including debris floods) in the area around Vassenden. In this paper, we focus on 52 of these shallow landslides from which the authors have direct and detailed field observations. The detailed documentation includes the local landslide history and climate, meteorological situation, a summary of the reported course of events, detailed geological characterisations of major 2019 landslide clusters, leading up to analyses of shallow landslide causes and triggers.

Geological setting, climate, and landslide history

The Jølster area is positioned in a long glacial valley on the western side of the South Scandinavian Mountain range (Fig. 2B). The east–west oriented inland valley is not connected with the maritime fjords, but large parts of the valley bottom are covered by lake Jølstravatnet, that together with its connected lake Kjøsnesfjorden stretches eastwards some 30 km towards the large ice cap Jostedalsbreen. The bedrock in the study area is dominated by various gneisses which are largely exposed in the higher parts of the landscape (1000–1100 masl) as a majority of glacially rounded surfaces but also some steeper bedrock scarps. On the upper slopes a thin cover (<0.5–1 m) of organic soils and grasses commonly drapes the bedrock. The mid- and lower slopes are largely covered with varying thin (<0.5 m) and thick (>0.5 m) cover of glacial till (Fig. 1A). The till often has a sandy-silty matrix composition and is relatively scarce in boulders. The valley bottom is mostly covered by glacial till, which in places is overlain by fluvial sediments or peat deposits (Fig. 1A). Slope process material is found on top of the till on some of the lower slopes: in the area around Vassenden (Fig. 1A) mass movement deposits consist mostly of rockfall debris under vertical bedrock sections, while alluvial fans in front of pre-existing debris-flow tracks are more common in the eastern reaches of lake Jølstravannet. The north-facing slopes leading down to Jølstravatnet (Fig. 1A, B) are cut by a multitude of long and incised debris-flow tracks. The age of these incisions is not known and since they lead into the lake, the potentially dateable deposits are under water.

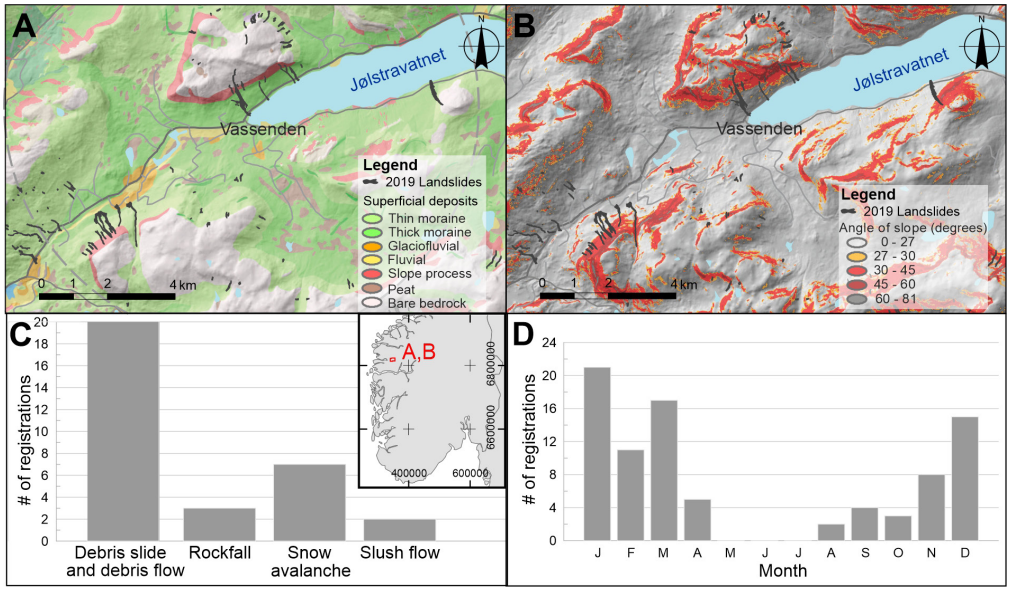

Figure 1. Geology and landslide history (A): Map showing superficial deposits with Jølster 2019 landslides (Lindsay et al., 2022). (B): Slope map with Jølster 2019 landslides (Lindsay et al., 2022); map frames A and B are located on the inserted map showing southern Norway. (C): 32 historical landslides in the Norwegian Mass Movement Database (NMMD) grouped by the mass movement type in the Vassenden region (7 km radius; indicated with grey dotted line in A). (D): 86 registered mass movement events (except rockfall) for a larger region around lake Jølstravatnet sorted by the month of the year.

The western part of Jølster has a maritime climate with winter temperatures just below 0°C at sea level. Mild winters with temperatures varying around 0°C often lead to rain-on-snow events and resulting slush flows are not uncommon around lake Jølstravatnet. Mean annual precipitation is 2300 mm, with most of the precipitation falling in autumn and winter (SeNorge, 2022). Heavy storms typically occur in this part of the year; at times with catastrophic consequences. Particularly the storms Loke (Nov 2005), Dagmar (Dec 2011) and Hilde (Nov 2013) led to several shallow landslides in the region, which is reflected by registrations in the Norwegian Mass Movement database (NMMD; NVE, 2019). The NMMD shows that shallow landslides are the most frequently reported mass movement types in the area around Vassenden (Fig. 1C). It is important to note that slush flows are often reported as snow avalanches or debris slides/flows in historical records and are believed to be underreported. One of the first records of multiple slush flow and landslide events around the lake Jølstravatnet is 28 January 1689 when severe damage was reported for 7 properties around Jølstravatnet and in Angedalen to the north. Several houses were swept away by the slush flows and 3 persons were killed in this historic event. When sorting registered mass movement events (except rockfall) from the 27 km-wide area around Jølstravatnet, Slåtten and Angedalen (the site of the 2019 event) by month, most events are observed from November to March (Fig. 1D). Landslides during summer are very uncommon in the historical records for the region.

For the landslide paths of 30 July 2019 (Fig. 1A, B), no previous events in the same paths were registered in the NMMD. Further research into written documentation and local sources has revealed several historical mass movement events in the affected areas (Hefre et al., 2019; Høydal & Sandersen, 2019). These historic events encompass rockfall and slush flows whilst none of the largest 2019 landslide paths had a well-known history of debris-flow activity. The river Årsetelva in Vassenden, which the debris flow *Tindefjellet 8* of the 2019 event (Figs. 2A & 3B) entered around 295 masl, already had mitigation measures against slush and debris in place to protect the settlement. The first were built in the 1960s with a deflection dam above the settlement. In 2016, erosion protection along the riverbed and riverbanks down through the settlement was completed and has prevented greater harm.

Hazard mapping on contract from NVE and according to the national system was carried out in parts of Jølster in 2018 and including the most populated areas in the municipality (Hefre et al., 2019). The Slåtten area, despite being a spread rural settlement, was not included in the hazard mapping in 2018 and was not mapped until autumn 2019, after the Jølster event (Høydal & Sandersen, 2019).

Meteorological situation in Jølster July 2019

July 2019 was warm and dry in western Norway prior to the event. As a consequence, the modelled groundwater levels were low to very low compared to normal in areas not directly affected by snow and glacier melt in the Scandinavian Mountains (xGeo, 2019a, b). Another consequence of the unusually warm summer were abundant local thunderstorms, illustrated by the fact that MET issued hazard warnings for torrential rain on approximately 30 days between May and September (NVE, 2020). On Tuesday 30 July 2019 and the following night, several torrential rain events and over a thousand strokes of lightning were registered in western Norway (Agersten et al., 2019).

During the week and weekend prior to the Jølster event, unusually warm air masses lay over southern Norway. On 29 and 30 July colder air masses approached from the east and northeast and created instabilities in the atmosphere which intensified as the air masses moved westwards and took up humidity over the glaciated and snow-covered areas of the South Scandinavian Mountains (Agersten et al., 2019). The municipality of Jølster was most severely affected by the resulting precipitation (NVE, 2019). The closest official meteorological station with an hourly precipitation record is runby the Norwegian Public Road Administration (SVV) and is situated in Vassenden, at the western end of the lake Jølstravatnet (Fig. 2B). For this station, the total rainfall the week prior to the event

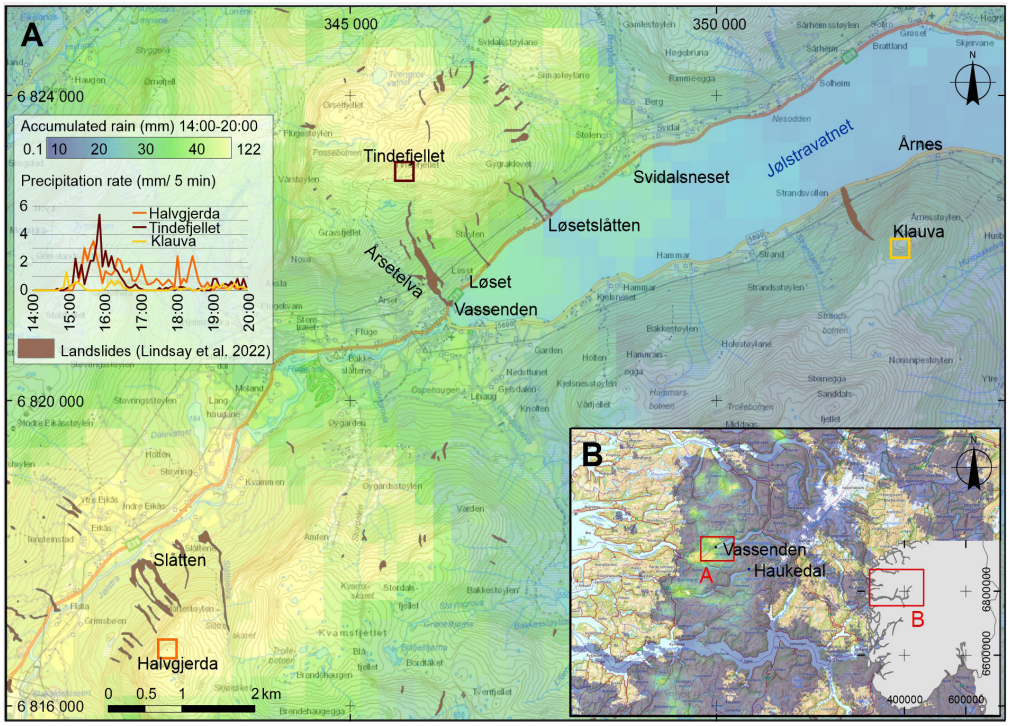

Figure 2. Meteorological situation based on weather radar at Vassenden (A) and in western Norway (B); map frame B is located on the inset map showing southern Norway. Areas of highest rain intensities show high correlation with occurrence of 2019 landslides (Lindsay et al., 2022). Maps A and B show rain accumulated from 2 to 8 pm on 30 July 2019, whereas the inserted graph shows precipitation rate in mm per 5 minutes for three selected grid locations at Halvgjerda, Tindefjellet and Klauva (indicated in map A with red, brown, and yellow box respectively). The locations of closest weather stations with hourly precipitation measurements are indicated in map B.

(23 to 29 July) amounted to 3.6 mm, while on 30 July the record shows no rain prior to 4 pm, and 33 mm between 4:00 and 4:53 pm when the precipitation sensor was swept away by a large debris flow (*Tindefjellet 8*; Fig. 2B). The second closest official station with hourly precipitation record, Haukedal, is situated 16 km SSE of lake Jølstravatnet (Fig. 2B). Here, a total of 113.6 mm rain fell from 30 July at 3 pm to 31 July at 2 pm (Agersten et al., 2019), a clear record high since the start of the time series in 1957, exceeding the 200-year event magnitude. Maximum precipitation intensity at Haukedal was reached between 7 and 8 pm in the evening of 30 July. However, reports by eyewitnesses and weather radar data suggest that the Jølster area around Vassenden experienced even more intense rainfall, peaking between 3 and 5 pm on 30 July (Fig. 2). Weather radar data has limitations due to shadow effects in the Western Norwegian rugged landscape (e.g., Abdella et al., 2012) and large uncertainties for calibration of extreme convective rainfall (Abdella et al., 2012; Elo, 2012; Ødemark et al., 2012). Yet, due to large spatial and temporal variations in rainfall intensity, weather radar still gives a more complete areal picture than precipitation interpolated from fixed stations with hourly measurements (cf., inserted graph in Fig. 2A which shows precipitation rate in mm per 5 minutes based on radar data for three selected points in the study area between 2 and 8 pm).

Course of events

The first report of a landslide affecting the main traffic route E39 along the northern shore of lake Jølstravatnet between Førde and Skei was reported to the western police district at 4:26 pm on 30 July (Kalajdzic & Folkman, 2019). According to this first report, debris and water blocked the E39 at Svidalsneset (Fig. 2A) causing the fire brigade to drive out to close the road. The emergency responders then were detained by debris and water blocking the road by the river mouth of Årsetelva in Vassenden (Fig. 2A). This led to initial confusion about the actual location of the first reported damage site. At 4:53 pm, more water and debris came down Årsetelva, damaging a cabin and endangering three residential houses. The area around the Årsetelva river mouth was evacuated, and at 4:58 pm it was confirmed that there were two separate damage sites, Svidalsneset and Årsetelva (Figs. 2A & 3B, D). Several landslides were then reported on the same stretch of road at Løsetslåtten (Figs. 2A & 3C) and in the rural settlement of Slåtten (Figs. 2A & 3A), west of the Vassenden village. Lower (eastern) Slåtten was affected by a flood in the Slåttelva river while eleven shallow landslides were released from the steep mountain side of Halvgjerda. Four of these shallow landslides reached farmland and endangered settlements: the first three subsequent shallow landslides released at around 4:30 pm reached the farmland of upper (western) Slåtten, before a fourth far-reaching landslide endangered the farm at middle Slåtten at 5:30 pm.

A total of four landslides crossed the E39 road and more than 150 people were evacuated. The landslides created power outages, disrupted telecommunications and traffic, and blocked people, ambulances and cars inside the area of the most far-reaching landslides. The county road Fv 5690 (then Fv 451) on the southern side of Jølstravatnet is the only possible detour road from Vassenden eastwards. This road was closed by the authorities during the period with most intense landslide activity (around 5 pm) but was opened in the evening when the rain in Vassenden had decreased. According to the district chief executive, non-residents were desperate to get out of the area and parents were in urgent need of picking up their children after school and leisure activities in surrounding communities (Reksnes & Grimeland, 2019). At 8:45 pm there was a new large landslide reported, this time on the southern side of Jølstravatnet, over the then opened Fv 5690 west of Årnes (Fig. 2A; Kalajdzic & Folkman, 2019). One car was reported to have been taken by the landslide. After 10–15 minutes, the fire brigade arrived by boat to the site and started searching. After yet a quarter of an hour, more help arrived from a helicopter and another boat. The search for the car was officially ended five months after the incident with the conclusion that one man died in this landslide. A total of 15 flood or landslide incidents were registered in western Norway on this day (NVE, 2019).

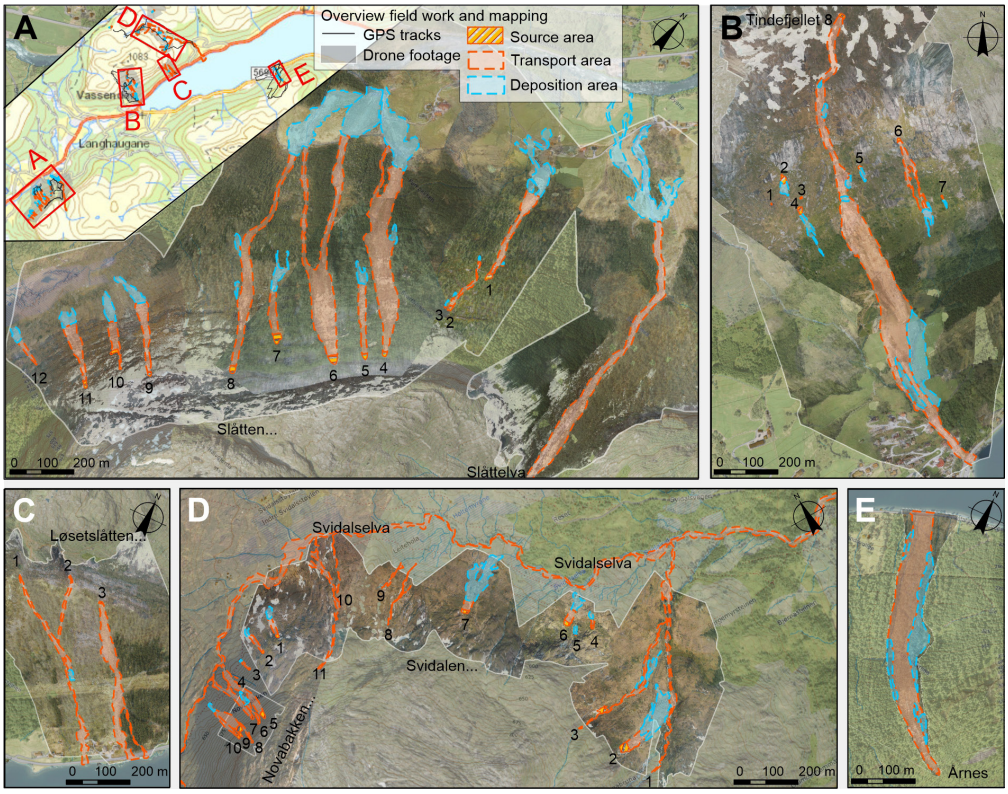

Figure 3. Detailed mapping presented in this study. Inserted overview map for the area around Vassenden locates maps A–E. (A): One debris flood in Slåtteelva, as well as debris flows and debris avalanches consecutively numbered as Slåtten 1–12. (B): One large debris flow Tindefjellet 8 alongside with minor debris flows, slides and slumps named Tindefjellet 1–7. (C): Two merging debris floods/flows and one debris flow at Løsetslåtten 1–3. (D): One debris flood with increasing downstream erosion in Svidalselva, Svidalen 1–11 and Novabakken 1–11 encompassing several debris floods in tributary streams, slumps, debris slides and flows; not represented in this map view are debris avalanches at Tverrgrovi and Storehola. (E): The fatal debris avalanche at Årnes.

Methods

Field mapping

Fieldwork was carried out over twelve days in the period between August 2019 and May 2021 (GPS tracks in overview map inserted in Fig. 3A). The largest landslides were mapped systematically with focus on characterisation of source, transport and depositional areas, where present. This includes the description of stratigraphy in scars and at selected locations along the landslide paths, estimation of width and erosion depth, description of sliding planes and characterisation of bedrock and sedimentary deposits. In addition, several of the smaller slumps and slides have been studied in detail.

Landslide mapping in GIS environment

On five of the field days in 2019, classical field mapping was accompanied by a drone survey conducted by HVL (Western Norway University of Applied Sciences). Drone imagery was converted to orthophotos using the Agisoft Metashape software and the ground resolution lies between 5 and 20 cm per raster pixel. To ensure time efficiency, the resulting orthophotos were not corrected based on ground-control points (GCPs); therefore, camera location errors are in the order of 0.3 to 1 m in the x and y directions. The orthophoto for Årnes was captured and rectified by NGI (Norwegian Geotechnical Institute) by the

use of GCPs with an achieved ground resolution of 1.76 cm per pixel. In addition, a DEM derived from the NGI drone campaign at Årnes was compared to Lidar-based DEMs from the Mapping authorities (Kartverket) from 2016 and 2017 with 0.5 m and 0.25 m resolution, respectively. Areas higher up on the hillslope were only covered during the 2016 Lidar-campaign and resampled in order to create a mosaic with 0.25 m resolution (before DEM). The before-DEM was then clipped to the extent of the drone-derived terrain model (after DEM). In a final step, altitude difference (*minus*) between the two DEMs as well as resulting volume changes (*cut fill*) were calculated in order to map and quantify erosion and deposition of this debris avalanche.

Since the drone surveys do not provide complete coverage for all landslides, Esri's satellite Imagery basemap was used as a support. The satellite scene of interest, Maxar WV02 27/08/2019, has 0.5 m resolution, yet only an accuracy of 8.47 m. Where drone imagery was lacking, the Maxar satellite imagery was therefore manually georeferenced for a better fit. Datasets used for remote sensing-based landslide mapping further included hillshade, slope and flow accumulation maps derived from the national DEM dataset with 1 m resolution by Kartverket. Range and mean slope for source, transport and deposition areas were calculated using zonal statistics. Furthermore, drop height and runout length were used as input to calculate alpha angles. These are only meaningful in cases where landslides do not hit standing water. A prototype of a newly developed NGU geological-landslide geodatabase was employed during mapping and the resulting dataset (in Norwegian language) is provided as open access (Electronic supplement 1).

Weather stations and radar data

The closest official rain gauges with hourly measurements are Vassenden at 210 masl and Haukedal at 311 masl (both stations are located in Fig. 2B). Whilst the records summarised in the paragraph *Meteorological situation in Jølster July 2019* are freely available, we also provide a copy of the relevant weather and climate data in the Electronic supplement 2.

Weather radars emit radio waves which get reflected as they hit precipitation per unit volume at a certain height above the ground. The weather radar data in this study are gridded with a spatial resolution of 250 m (presented in Fig. 2) and were provided by MET. They were delivered as Net Channel Definition Format (CDF) scenes corresponding to rain intensity in mm/ 5 minutes and accumulated rain in mm from 2 to 8 pm. Western Norway is covered by five Doppler C-band weather radars, two of which were dual polarization systems in July 2019. Most uncertainty and errors in rainfall estimations from radar data can be explained with the vertical variability of the radar signal due to radar signal phase changes and different types of precipitation (Elo, 2012). To convert radar reflection (Z) to precipitation intensity (R) the Marshall-Palmer relation is employed

$$Z = aR^b$$

where parameters a and b depend on the type of precipitation, and standard empirical values for summer rain are a=200.0 and b=1.6 (Abdella et al., 2012; Elo, 2012). The radar data used are filtered but not corrected for measured precipitation values, nor is the vertical variability incorporated in the radar equation by means of Vertical Profile of Reflectivity (VPR).

Results

Shallow landslides at southern Tindefjellet

This location is dominated by a large debris flow which destroyed infrastructure, endangered several houses and blocked the main E39 road along its path down to the lake Jølstravatnet at 207 masl (Figs. 2A, 3B & 4; *Tindefjellet 8* in Table 1). In the source area at 875 masl (Fig. 4A), the sediment depth at the backscarp varies from 10 to 60 cm of organic turf and podsol (Fig. 4B, D). The sliding plane is partly developed on bedrock, whilst pockets of weathered and unweathered till withstood erosion (Fig. 4B). One metre above, and parallel to the backscarp, an open fissure in the vegetation cover was observed after the event (Fig. 4C). One boulder could be identified 10 metres below the backscarp on pre-event aerial photos and was moved 15 metres downhill by the event, where it was deposited on top of smaller-sized rocks and boulders in the central part of the flow path.

At 295 masl the debris flow confluences with a debris flood in the river Årsetelva. This debris flood was highly erosive, in particular just before the confluence point where it eroded 2 metres deep into sedimentary deposits. Erosive forces intensified as the debris flood and flow joined, and from 265 masl the two landslide paths into a 3–4 metres-deep and maximum 25 metres-wide channel along Årsetelva, with levees locally 1–2 metres in height.

Seven smaller debris flows, debris slides and slumps occurred at Southern Tindefjellet (Figs. 3B & 4; Table 1). Our observations at this location and in Svidalen suggest the failure mechanism to be slumping where the failing material consisted of thin grass-bound topsoil (0.05–0.1 cm), whereas sliding was more common where soil profiles were in the order of 0.5–1 metre thick. The source areas are all situated above the forest line where vegetation is dominated by grass, heath and berry bushes with sporadic birch trees. Three weeks after the event, abundant signs of surface runoff and erosion could be seen at this location, also outside the landslides themselves. This included flattened grass, terrestrial and plant debris deposited by surface overland flow, as well as small-scale failures and slumps of grass-bound topsoil. None of the shallow landslide scars adjoin permanent streams and they accumulate runoff from moderately sized upstream areas (ranging from 2 500 to 13 000 m^2; Table 1).

Table 1 Summary of geomorphological and geological characteristics for the mass movements at location Southern Tindefjellet

	Source point/ area masl	Slope source area (°)	Drop height (m)	Alpha angle (°)	Acc. flow (m^2)	Scarp sediment depths (m)	Cliff above	Process
Tindefjellet 1	573	29–36 (32)	7	26.6	6 366	0.05–0.1 (0.1)	no	slump
Tindefjellet 2	618	20–45 (32)	40	29.7	8 076	0.2–0.7 (0.4)	medium	slump
Tindefjellet 3	581	23–57 (42)	8	28.1	7 299	0.2–0.5 (0.3)	no	slump
Tindefjellet 4	563	13–47 (27)	100	29.3	5	0.2–0.7 (0.5)	no	debris flow
Tindefjellet 5	592	21–51 (37)	39	37.4	4 235	0.4–1.0 (0.8)	minor uphill	debris slide
Tindefjellet 6	629	20–41 (33)	212	33.5	2 593	0.05–0.5 (0.2)	minor	debris flow
Tindefjellet 7	483	29–55 (41)	30	34.9	2 583	no observation	no	debris slide
Tindefjellet 8	875	22–55 (34)	668	23.1	13 132	0.1–0.6 (0.4)	minor uphill	debris flow

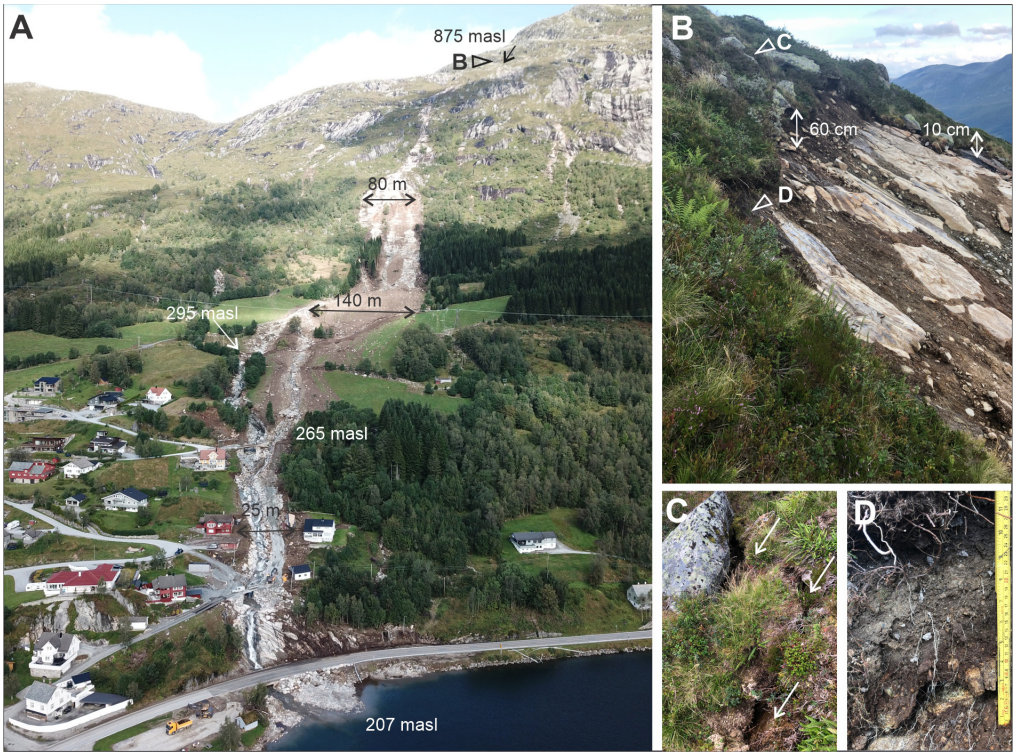

Figure 4. Vassenden or Årsetelva debris flow (referred to as Tindefjellet 8 in this study) (A): Birds-eye view illustrates the widening to 80 metres width over two cliff sections from 600 to 350 masl and further to a maximum width of 140 metres between 350 and 275 masl before getting channelized for the last 50 metres of drop height. (B): Source area of Tinde-fjellet 8, with scarp sediment depth and indication of where photos in C and D are taken. (C): Fissure one meter above and parallel to the backscarp. White arrows indicate potential water infiltration. (D): Soil profile in the backscarp with a 10 cm thick leached layer (E horizon).

Shallow landslides at Løsetslåtten

At this location, two debris floods/flows joined paths after 150 metres of drop height and another, wider, debris flow endangered the settlement and blocked the main E39 road (Figs. 3C & 5). All three initiated at the bottom of an at least 200 metres-high cliff (Fig. 5A). While the western debris floods/flows (*Løsetslåtten 1* and *2*) follow pre-existing channels and drain more than 50 000 and 10 000 m^2 of terrain, respectively, the source area of the eastern debris flow (*Løsetslåtten 3*) receives surface runoff from roughly 2 400 m^2 (Table 2). Based on drone photos the scarp sediment depth for the eastern debris flow varies from grass-bound topsoil of a few centimetres in contact with the bottom of the cliff, to half a metre of boulder-rich topsoil. The flow path widened to 45 metres in the upper part, while becoming more confined due to a pre-existing channel in the lower part. At 250 masl, part of the masses were deflected into a second pre-existing channel to the east, presumably preventing damage to the residential house at this location. The *Løsetslåtten 3* flow path was not identified in neither susceptibility nor hazard zone maps (Hefre et al., 2019). Large boulders were observed in spruce forest by the road northeast of the lowermost part of the debris-flow path.

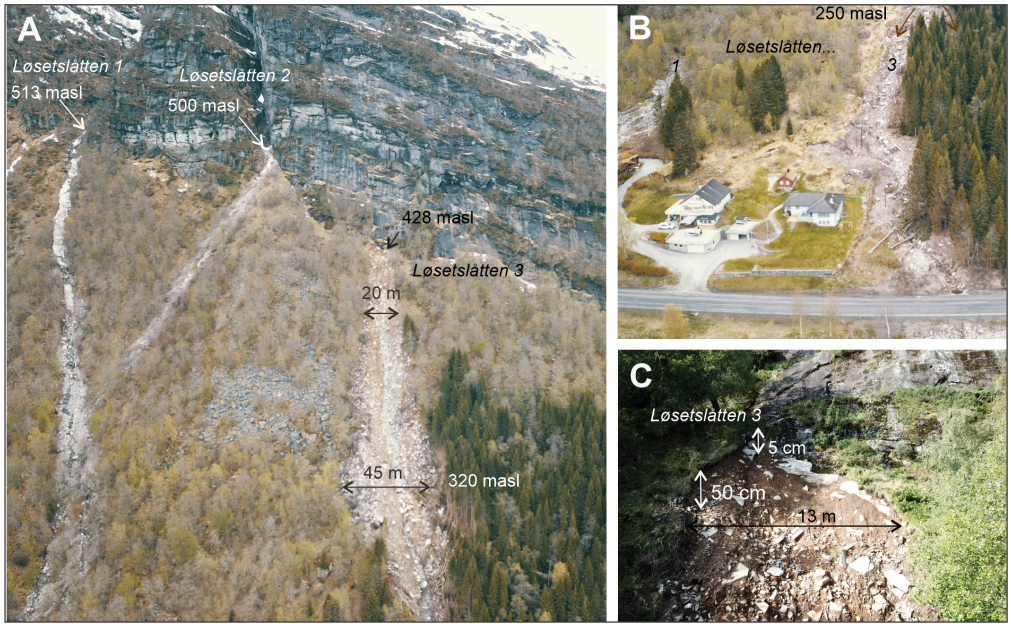

Figure 5. Two merging debris floods/flows and a debris flow at Løsetslåtten (A): 200-metres-high cliff over the source areas at 513, 500 and 428 masl respectively. (B): Settlement endangered from two sides at the lower part of the transport areas; lake Jølstravatnet is situated just beyond the road. (C): Source area of the debris flow Løsetslåtten 3 with indication of scarp sediment depth and initial width.

Table 2 Summary of geomorphological and geological characteristics for the mass movements at location Løsetslåtten

	Source point/ area masl	Slope source area (°)	Drop height (m)	Alpha angle (°)	Acc. flow (m²)	Scarp sediment depths (m)	Cliff above	Process
Løsetslåtten 1	513	no source area	306	25.6	53 416	no backscarp	major	debris flood/flow
Løsetslåtten 2	500	no source area	150	35.3	11 029	no backscarp	major	debris flood/flow
Løsetslåtten 3	428	31–63 (43)	220	23.5	2 404	0.05–0.5 (0.3)	major	debris flow

Shallow landslides in Svidalen

A debris flood affected the river Svidalselva, damaged public infrastructure, private property and blocked the main E39 road at the river mouth at Svidalsneset. Whilst not destroying or endangering any infrastructure, a total of 12 small debris slides, avalanches, slumps and debris floods occurred in the valley of Svidalen, on the eastern slope of Tindefjellet (Figs. 2A, 3D & 6). The debris floods occurred in small tributaries to the stream Svidalselva. They involve erosion of weathered bedrock, in particular over steeper passages between 600 and 550 masl (>35 degrees), as well as undercutting of regolith and subsequent overturning (Fig. 6C) or slumping (Fig. 6E) of the grass-bound topsoil in gentler terrain between 550 and 500 masl (<30 degrees). Deposits built up in mounds on alpine meadows as slope angles drop to below 20 degrees (Fig. 6A, B). The debris avalanches and debris slides are all situated beneath minor cliffs or exposed bedrock, have moderate flow accumulation values and highly variable scarp sediment depths (Table 3). Just as for the large debris flow at *Vassenden 8*, an open fissure in the vegetation and upper soil could be observed one metre above and parallel to the backscarp debris slide *Svidalen 4* (Fig. 6D). The source areas of debris avalanches *Svidalen 2* and *7* (Fig. 6F, G) are in part eroded down to the bedrock, whilst in part the sliding plane is developed in grey or brown diamict.

Figure 6. Debris floods, slides, avalanches and slumps in Svidalen (A, B): Debris floods; examples of deposition of material in mounds on alpine meadows. (C): Example of undercutting of regolith and overturning of grass-bound topsoil. (D) Debris slide which partly slid down a ledge, partly remained on top of the ledge. (E): Slumped grass-bound topsoil. (F, G): Two small debris avalanches with highly variable scarp sediment depth and character, partly eroded down to the bedrock.

Table 3 Summary of geomorphological and geological characteristics for the mass movements at location Svidalen, eastern Tindefjellet

	Source point/ area masl	Slope source area (°)	Drop height (m)	Alpha angle (°)	Acc. flow (m^2)	Scarp sediment depths (m)	Cliff above	Process
Svidalselva	637	no source area	431	6.1	5 379	no backscarp	no	debris flood
Svidalen 1	675	no source area	240	13.5	533 820	no backscarp	minor	debris flood
Svidalen 2	607	14–46 (31)	81	17.3	7 536	0.5–1.5 (1.0)	minor uphill	debris avalanche
Svidalen 3	600	15–47 (29)	163	19.1	3 826	0.05–0.2 (0.1)	no	debris flood
Svidalen 4	515	23–57 (34)	21	20.9	6	0.5–1.3 (0.8)	minor uphill	debris slide
Svidalen 5	525	37–48 (43)	19	28.5	2 809	0.4–1.0 (0.6)	minor uphill	debris slide, slump
Svidalen 6	515	17–43 (30)	28	15.6	1 062	0.1–0.9 (0.4)	minor uphill	debris slide
Svidalen 7	556	22–36 (30)	56	13.9	3 135	0.2–1.2 (0.8)	minor	debris avalanche
Svidalen 8	557	9–34 (22)	79	19.8	9 984	0.1–0.7 (0.4)	no	debris flood, slump
Svidalen 9	550	no source area	31	16.4	87 880	no backscarp	no	debris flood
Svidalen 10	572	no source area	42	11.4	2 250	no backscarp	no	debris flood
Svidalen 11	578	no source area	127	15.4	172 261	no backscarp	no	debris flood

Shallow landslides at Novabakken

At Novabakken on the northern slope of Tindefjellet, several superficial debris slides and flows as well as two rockfalls and a debris flood were identified from the 2019 Jølster event (Figs. 2A, 3D & 7). The debris avalanches at Tverrgrovi (Fig. 7C, D) and Storehola are also included in this summary (Table 4). Souce areas are generally very steep (>35 degrees) and coarse-grained consisting of scree with soil development. In some source areas, thin soil was eroded down to protruding bedrock, but most debris slides and flows are very superficial as grass and bushes in the landslide paths frequently withstood erosion. Debris flows at Novabakken have the highest drop heights of around 100 metres and follow pre-existing channels developed in thick weathered material. For several of the debris flows and slides the surface area draining to the source area is very limited (mostly well below 500 m^2, Table 4). Source areas at these locations were not observed directly but from drone footage.

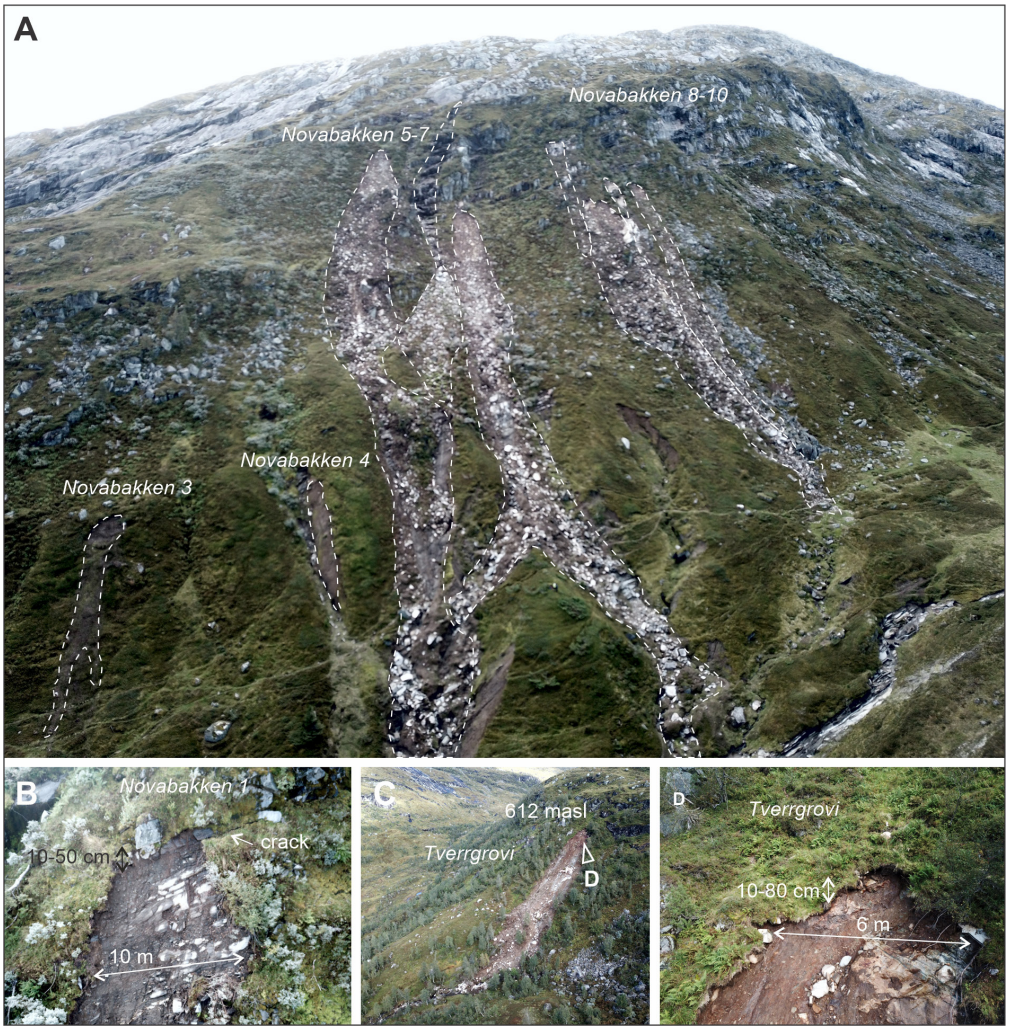

Figure 7. Superficial debris slides and flows at Novabakken and debris avalanche at Tverrgrovi. (A): Birds-eye view of debris slides and flows Novabakken 3–10. (B): Source area of a small debris flow at Novabakken 1 with a crack extending to the west from the backscarp. (C, D) Birds-eye view and source area of a small debris avalanche at Tverrgrovi.

Table 4 Summary of geomorphological and geological characteristics for the mass movements at locations Novabakken, (northern Tindefjellet), Tverrgrovi and Storehola

	Source point/ area masl	Slope source area (°)	Drop height (m)	Alpha angle (°)	Acc. flow (m^2)	Scarp sediment depths (m)	Cliff above	Process
Novabakken 1	620	38–55 (45)	66	32.4	15	0.1–0.5 (0.3)	minor	debris slide
Novabakken 2	625	31–52 (39)	66	34.5	2 844	0.1–0.5 (0.3)	minor	debris slide
Novabakken 3	630	34–48 (43)	30	33.7	1 308	0.05–0.3 (0.2)	no	debris slide
Novabakken 4	615	39–54 (49)	32	25.5	5 470	0.01–0.1 (0.05)	no	debris slide
Novabakken 5	725	29–58 (39)	141	32.1	110	0.1–0.6 (0.25)	minor	debris flow
Novabakken 6	728	27–62 (50)	86	35.2	17 460	no observation	minor	rock/debris fall
Novabakken 7	700	35–45 (40)	106	30.2	69	0.1–0.8 (0.4)	minor	debris flow
Novabakken 8	758	20–58 (31)	68	40.4	193	no observation	minor	rock/debris fall
Novabakken 9	714	31–55 (40)	94	32.4	1 904	no observation	minor	debris flow
Novabakken 10	714	33–45 (39)	94	32.8	120	no observation	minor	debris flow
Novabakken 11	660	no source area	32	13.1	107 040	no backscarp	no	debris flood
Tverrgrovi	612	32–55 (39)	70	26.6	869	0.1–0.8 (0.4)	minor uphill	debris avalanche
Storehola	650	34–46 (40)	74	34.8	360	0.1–0.5 (0.3)	minor	debris avalanche

Shallow landslides at Slåtten

A debris flood in the stream Slåttelva led to substantial erosion along the riverbanks and sediment deposition on the farmlands of lower Slåtten (Fig. 3A). In addition, several debris flows and debris avalanches were released on the northern slope of the mountain Halvgjerda (Figs. 2A & 3A). Most of the landslides at this location have very steep source areas (>35 degrees on average), receive surface runoff from small to moderate upstream areas (<10 000 m^2) and lie underneath cliffs of varying size (Table 5). To the northeast, a debris flow with 203 metres drop height threatened a farm at middle Slåtten (*Slåtten 1* and *2*; Table 5; Figs. 3A, 8B–D), while three others with drop heights between 425 and 480 metres reached farmlands of upper Slåtten (*Slåtten 4, 6* and *8*; Table 5; Figs. 3A, 8E–H).

Above the settlement middle Slåtten, two small debris slides *Slåtten 2* and *3* and the large, main debris flow *Slåtten 1* were released at around 5:30 pm. *Slåtten 3* is an isolated debris slide with short runout, but a causal relationship between debris slide *Slåtten 2* and debris flow *Slåtten 1* was recognised during fieldwork, highlighting the importance of waterpaths and blockages by trees for downslope entrainment of debris (Fig. 8B). The failed topsoil of debris flow *Slåtten 1* is 10–60 cm thin (see Fig. 8C; Table 5), resulting in an estimated initiation volume of 95 m^3. The uppermost transport area consists of a cliff passage with an average slope of 42 degrees over 50 metres of drop height. Despite limited initiation volume and thin sediment cover in this upper transport area, the debris flow built up sufficient momentum to sustain channelised flow and erosion capacity through a gentler-sloped dense spruce forest (27 degrees on average), possibly due to the contribution of debris slide *Slåtten 2*. A substantial percentage of the total *Slåtten 1* landslide volume consists of eroded timber, which finally came to rest on farmland with 7 degrees average slope, less than one metre from the nearest property (Fig. 8D).

At upper Slåtten, eyewitnesses filmed while debris flow *Slåtten 6* reached their farmlands, at which point *Slåtten 4* had already been deposited, while *Slåtten 8* followed shortly after (see Figs. 3A & 8A for location); all of these events were officially registered at 4:30 pm. These three debris flows were released at the foot of Halvgjerda cliff between 574 and 592 masl (Table 5). In the upper steep transport areas (42 degrees), debris flows *Slåtten 4, 6* and *8* widen to 68, 72 and 40 metres, respectively.

Table 5 Summary of geomorphological and geological characteristics for the mass movements at the location Slåtten

	Source point/area masl	Slope source area (°)	Drop height (m)	Alpha angle (°)	Acc. flow (m^2)	Scarp sediment depths (m)	Cliff above	Process
Slåtteelva	574	no source area	434	15.2		no backscarp	no	debris flood
Slåtten 1	353	9–66 (35)	203	22.1	21 060	0.1–0.8 (0.3)	medium uphill	debris flow
Slåtten 2	429	29–43 (37)	143	34.5	2 774	0.1–0.6 (0.2)	medium	debris slide
Slåtten 3	424	33–42 (38)	18	34.3	614	0.1–0.3 (0.2)	medium	debris slide
Slåtten 4	574	17–39 (31)	425	26.8	1 415	0.5–1.2 (0.7)	major	debris flow
Slåtten 5	584	10–43 (31)	268	40.8	923	0.1–0.5 (0.2)	major	debris flow
Slåtten 6	592	23–54 (39)	480	23.6	536	0.1–0.35 (0.25)	major	debris flow
Slåtten 7	490	23–52 (39)	180	31.0	1 626	no observation	minor	debris flow
Slåtten 8	578	25–58 (38)	426	23.1	8 863	no observation	major	debris flow
Slåtten 9	572	27–48 (36)	275	38.2	1 717	no observation	major	debris avalanche
Slåtten 10	545/500	35–62 (48) 32–39 (35)	125	29.6	1 130 1 627	no observation	major	debris avalanche
Slåtten 11	570	26–63 (44)	165	32.9	761	no observation	major	debris avalanche
Slåtten 12	395	no source area	100	35.5	3 630	no backscarp	major	rock/debris fall

In the lower transport area through gentler sloped (25 degrees) deciduous and spruce forest, the *Slåtten 4* and *6* paths both split in two branches (Fig. 8A). For the broader eastern branch of *Slåtten 4*, deep erosion down to the bedrock or down to pockets of grey consolidated diamict is restricted to two pre-existing channels, while only roughly half a metre of the topmost 1–2 metres of brown diamict was eroded in the mid-section between those channels. In the lowermost transport area, the path of *Slåtten 6* eroded deeply into the sediments and revealed a stratigraphy of 1–1.5 metres of grey consolidated diamict, layered in places, overlain by 1.5–2 metres of brown, less compact diamict (Fig. 8G shows the eastern branch). The lower transport area of *Slåtten 8* (20 degrees) is funnelled into a pre-existing channel eroding up to 4 metres deep into grey and brown diamict (Fig. 8H). The deposition area of the debris flow *Slåtten 4* came closest to the farm buildings at upper Slåtten and consists of a first pulse with coarser material where fallen logs are again an important component of the total volume. The logs have functioned as a plug, stopping the first debris flow pulse of coarse material, and forcing the second pulse of finer material to turn westwards, away from the farm building (Fig. 8F). As mentioned, the deposition of *Slåtten 6* is caught on video and the first pulse with coarser grained material reaches the farmlands simultaneously from both channels. The material deposited by *Slåtten 8* is coarser and superimposed on deposits from the western branch of debris flow *Slåtten 6*. Erosion from this event created a channel through the depositional area on the farmland which reveals a 2 metres-deep soft-sediment cover which will be discussed under *Characteristics of landslide deposits*.

Debris flow *Slåtten 5* has a particularly small starting volume released at the foot of Halvgjerda cliff and does not reach farmland (Fig. 8A; Table 5). Debris flow *Slåtten 7* is released from a ledge roughly 100 metres of drop height below the foot of Halvgjerda cliff and stops in gentle-sloped mixed forest after 180 metres of drop height (Fig. 8A; Table 5). The three westernmost debris flows/slides and a rock fall (*Slåtten 9–12*; Figs. 3A & 8A; Table 5) have short runouts towards the bog Tjørnamyra and do not threaten any settlement. Based on drone photos, their deposits consist of coarse-grained material.

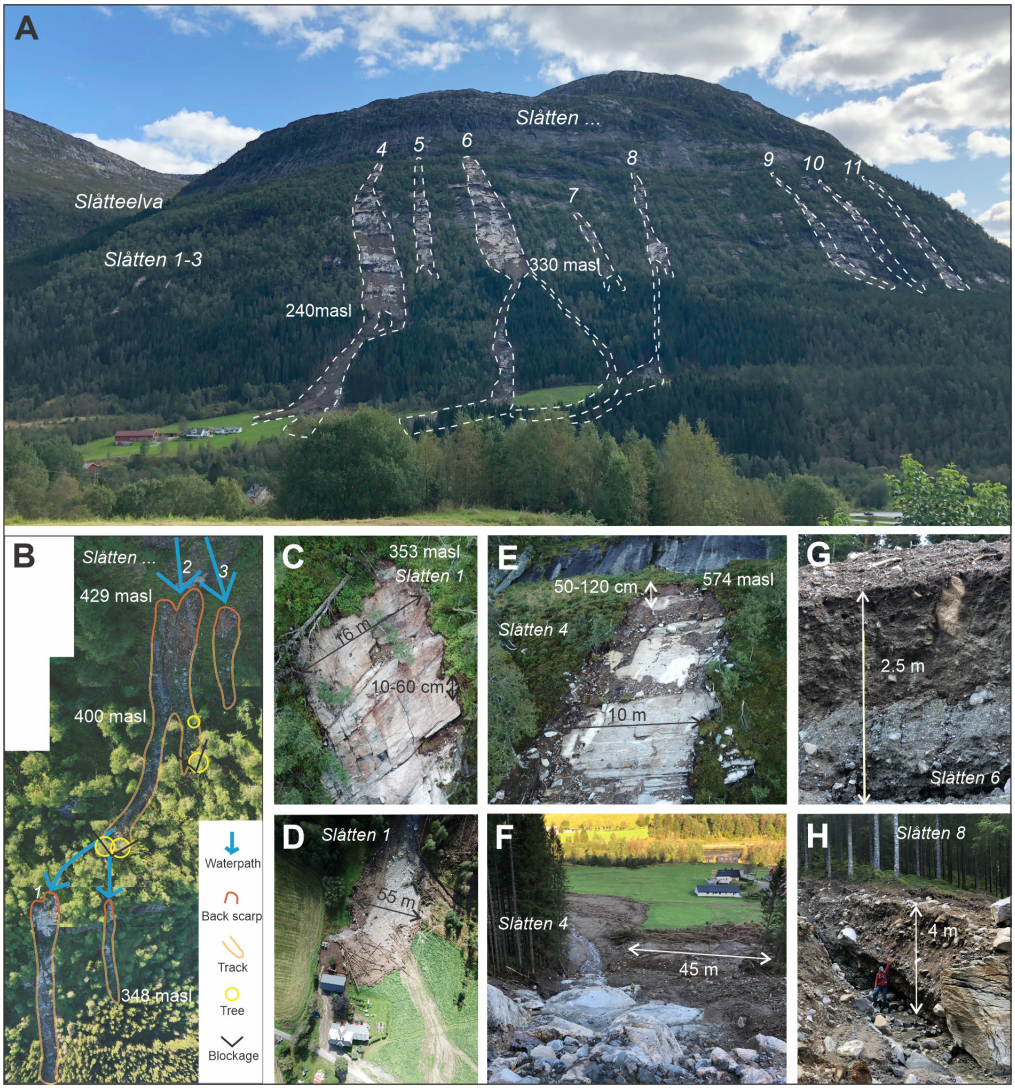

Figure 8. Debris flows at Slåtten (A): Overview photo showing the location of Slåtteelva and shallow landslides Slåtten 1–11. Debris flows Slåtten 1, 4, 6 and 8 reached farmland and receive special attention. (B): Complex trigger situation for debris flows Slåtten 1 and 2 where water paths and blockages by overturned trees were observed to play a key role. (C, D): Source and deposition area for debris flow Slåtten 1 at middle Slåtten. (E, F): Source and lower transport/ deposition area for debris flow Slåtten 4 at upper Slåtten. (G, H): Channel erosion in lowermost transport area of debris flows Slåtten 6 and 8 at upper Slåtten revealing a stratigraphy of 1–1.5 metres of grey consolidated diamict, layered in places, overlain by brown, less compact diamict of varying thickness.

Shallow landslide at Årnes

The source area is situated at the contact between protruding bedrock and thin podsoil cover, with 0.5 metre scarp depth on average, and drains a moderate upstream area of just under 3 000 m^3 (Fig. 9A, B; Table 6). Convex terrain, a minor cliff upslope and vegetation consisting of grass, heath, moss, fern and spread mountain birch characterise the source area. The sliding plane developed in brown diamict initially (Fig. 9B), before eroding down to the bedrock over a ledge and into a fine sand pocket following the ledge (Fig. 9A1). As documented in Fig. 9A, the track widens steadily: i) From 650 to 520 masl over steep cliff sections (35–45 degrees) where erosion mostly encompassed grass-bound topsoil. ii) From 520–400 masl over a slightly gentler sloped passage (30–35 degrees) with a thicker soft-sediment cover where erosion down to the bedrock was restricted to two main channels leaving a tree-covered island untouched in the uppermost part. iii) Below this island, a rockfall talus existed prior to the event; corresponding boulders were remobilised and deposited in a particularly coarse levee along the eastern flank of the debris avalanche from 400–310 masl (Fig. 9A3). iv) From 400–207 masl, through a

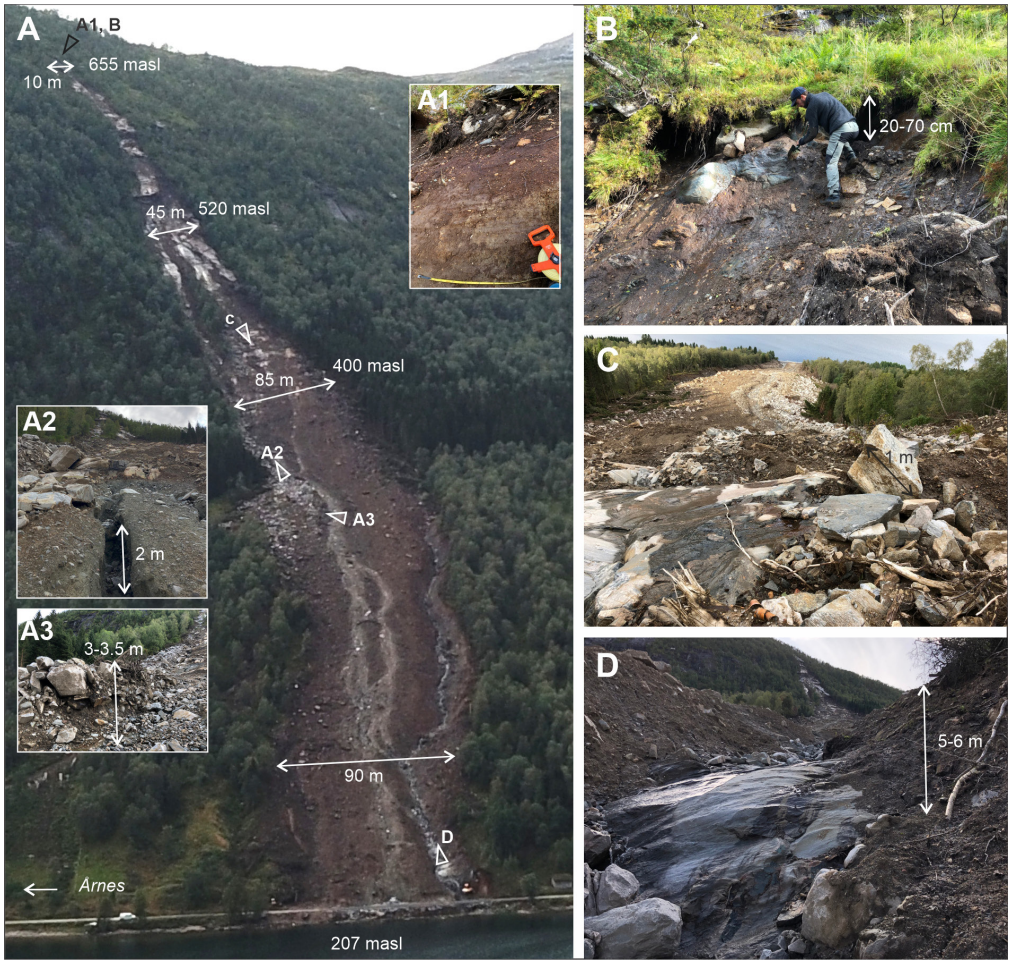

Figure 9. Debris avalanche at Årnes (A) Bird's eye view illustrates the widening to 45 metres and 85 metres width over two subsequent cliff sections (650–520 masl and 520–400 masl) and indicated where photos A1–A3, B, C were taken. (A1): Sliding plane in fine sand pocket. (A2): Channel eroded into soft sediment cover reveals that general erosion surface is 10–50 cm above the lithological boundary between grey and brown diamict. (A3): A particularly coarse levee due to a remobilized rockfall talus. (B): Source area at 655 masl. (C): Lower transport area with relatively constant width of around 80–100 metres. (D): Erosion down to the bedrock in pre-existing channel on the western flank of the debris avalanche.

Table 6 Summary of geomorphological and geological characteristics for the mass movement at location Årnes

	Source point/ area masl	Slope source area (°)	Drop height (m)	Alpha angle (°)	Acc. flow (m^2)	Scarp sediment depths (m)	Cliff above	Process
Årnes	655	33–44 (38)	448	27.8	2 991	0.2–0.7 (0.5)	minor	debris avalanche

more gently sloped belt of spruce and mixed deciduous forest (15–25 degrees) the track width varies between 80 and 100 metres (Fig. 9C), while estimated pre-event soft-sediment cover gradually increases from 2–3 to 5–6 metres (Fig. 9D). Erosion down to the bedrock in this lower transport area is limited to one main pre-existing channel on the western flank (Fig. 9A, D). In the remaining area, various shallower channels have eroded into the soft-sediment cover following the event, revealing a stratigraphy which consists of grey consolidated diamict overlain by brown and looser diamict (Fig. 9A2). Observed thicknesses for both units vary largely from 0.5 to 2 metres depending on bedrock morphology and downslope position. Interestingly, the erosion surface over large parts of the lower transport area does not correspond to the vertical transition from lower consolidated grey to upper loose brown diamict, but is instead situated 10–50 cm above this lithological boundary (Fig. 9A2).

The comparison of pre- and post-event DEM shows that the central part of the landslide is characterised by net erosion along its entire length (corresponding to total erosion volume of 35 374 m^3), while net deposition is concentrated on the western narrow flank and eastern broader flank which make up for a net gain of 33 871 m^3. The total measured erosion is therefore restricted to 1 503 m^3. Depositional height exceeds 10 metres in places on both flanks, the eastern levee with remobilised boulders clearly makes up for one focus area of deposition. The deepest erosion in the order of 2 metres occurs in the western broader channel from 520 to 380 masl, while erosion only exceeds 50 cm sporadically above 520 masl and in narrow channels below 380 masl. For most areas that experienced net loss, the erosion depth is restricted to less than 20 cm.

Discussion

There is an evident link between the occurrence of extreme precipitation as indicated by weather radar data and the triggering of numerous landslides. In the following, we explore the meteorological trigger and release mechanism in greater detail as well as discuss the characteristics of the presented landslides in their source, transport and depositional areas.

Meteorological trigger

July 2019 was exceptionally dry and warm and the modelled water level for the study area was low to very low compared to normal (xGeo, 2019a, b; Electronic supplement 2). On 30 July the SVV weather station at Vassenden registered no rain prior to 4 pm and 33 mm between 4:00 and 4:53 pm when the precipitation sensor was destroyed by a debris flow (*Tindefjellet 8*; Fig. 3B). The onset of rain based on the weather radar data is approximately one hour too early compared to direct observations. This is due to the rain being measured at some height above the ground while most humidity vapourises without reaching the ground in the early phase of a convective rainfall with high air temperatures. Even though precipitation estimated from weather radar therefore overestimates the amount of precipitation in the early phase of the torrential rainfall, it still gives a more complete picture of the temporal and spatial variations of the event than direct measurements. With the exception of the late debris avalanche at Årnes which reached the road at 8:45 pm, all other shallow landslides which reached or endangered roads and settlements, happened in a small time window between 4:30 and 5:30 pm.

We calculated the local water supply threshold following Sandersen et al. (1997; first three columns in Table 7) based on duration of the precipitation until landslide release and the known mean annual precipitation for the area. The empirical equation by Sandersen et al. (1997) is mainly based on daily precipitation values and this calculation of critical water supply is therefore not well suited for precipitation with short durations. In the lack of a more updated equation for Norwegian conditions, we nevertheless compare this critical water supply with the amount of accumulated precipitation until the first landslide registration, based on weather radar data (Fig. 2; last two columns in Table 7). We note that accumulated rain at Halvgjerda (mountain above Slåtten) and Tindefjellet (mountain above Vassenden) by far exceeded the critical water supply. Both these locations were the focus of slope failures and witnessed numerous shallow landslides. At Klauva (mountain above Årnes) on the other hand, the measured water supply did not quite reach the calculated critical value. The fatal debris avalanche at Årnes thus did not follow the same pattern as other failures on this day, which were released shortly after highly intense rainfall.

Table 7 Critical precipitation until first registered landslide for three of the most severely affected areas calculated following Sandersen et al. (1997)

	Duration of precipitation D	**Critical water supply in % of mean annual precipitation, P = 1.2 * D0.6**	**Critical water supply amount in mm, R = (2300 mm) * P**	**Accumulated rain until first landslide from weather radar**	**Measured water supply relative mean annual precipitation**
Halvgjerda (Slåtten)	1.4 h	1.478%	33.994 mm	150.6 mm	6.5%
Tindefjellet (Vassenden)	1.8 h	1.726%	39.698 mm	204.6 mm	8.9%
Klauva (Årnes)	8 h	4.178%	96.094 mm	84.4 mm	3.7%

Release mechanism

In a recent study, Bondevik & Sorteberg (2021) explored groundwater level and temperature fluctuations in response to water infiltration by rain and snow melt on a hillslope in Anestølen, Western Norway. Bondevik & Sorteberg's (2021) 4 year-long record included the autumn storm Hilde on 15–16 November 2013 during which a debris flow was released on the monitored slope and showed that: i) Groundwater levels on slopes drop relatively quickly when water infiltration ceases, resulting in a small window of 4 to 5 hours during which a slope is in a critical state for a landslide to be triggered. ii) Since groundwater peaks as high as during the Hilde event occurred without triggering any landslides on the monitored slope, landslide release is likely determined by a slope-specific groundwater level threshold combined with the rate at which groundwater is raised. In Norway, precipitation-triggered landslides during spring and autumn storms seem to follow a general pattern where the trigger moment postdates the peak in precipitation intensity by 4 to 5 hours (e.g., as shown during the storm Loke 14 November 2005; Bondevik & Aa, 2014). Deploying these observations on the Jølster case, it is highly questionable whether the time from precipitation onset to release of most of the debris flows – a matter of 1 to 2 hours – was sufficient to transform soil with low and very low water contents into saturated soil profiles. It is therefore more reasonable to suggest that the trigger mechanism for most shallow landslides in Jølster was instead locally high porewater pressure caused by very intense rainfall and hence surface runoff, which penetrated into pre-existing fissures in the soil and at soil-bedrock or soil-boulder contacts. At several source areas, fissures were observed post-slide, either parallel, roughly 1 metre above the backscarp (e.g., the large debris flow in Vassenden *Tindefjellet 8* and debris slide *Svidalen 4*) or in lateral continuations of the backscarps (e.g., *Novabakken 1* and *Tverrgrovi*). It cannot be ruled out that these fissures opened post-failure and indicate the initiation of retrogressive failure. However, we hypothesise that they have opened pre-slide, due to the prolonged warm and dry weather in July, and subsequently facilitated rapid water infiltration and very localised build-up of water pressure. A recent master thesis by Larsen (2021) found that the numerical model TRIGRS did a poor job in reproducing the triggering of the Jølster shallow landslides. TRIGRS reproduces the build-up of porewater pressure either from a saturated or unsaturated state (Schilirò et al., 2021) considering time-dependent rainfall as input, which was estimated by the same weather radar data presented in this study (Fig. 2). The fact that the model failed to predict known source areas (Larsen, 2021), strengthens the hypothesis that the soil was not fully saturated at the point of failure and that porewater pressure instead had built up locally through infiltration in fissures. If this is the case, the triggering of extreme precipitation induced landslides following a dry spell or drought may generally not qualify for modelling in TRIGRS.

Landslide categorisation and source area characteristics

Field observations enabled the differentiation into three Jølster landslide categories, namely debris flows, debris slides and slumps. Debris flows started either as slides or slumps, and in places through riverbed erosion. Where soil merely consisted of a grass-bound topsoil, slumping was observed as the trigger, whereas sliding occurred in slightly deeper soils of 20 to 150 cm thickness. Whilst cohesion in clay-rich soils commonly prevents slumps from translating directly into debris flows (Iverson et al., 1997; Gabet & Mudd, 2006), slumps observed in this study consist of grass-bound sand-rich soil which is prone to disintegrate, liquify and thus develop into debris flows. Observations in Svidalen and southern Tindefjellet suggest that whether a failure results in a debris slide/slump or instead develops further into a debris flow depends on i) reaching a critical initial volume (e.g., not the case for debris slide/slump *Svidalen 5*) and ii) a sufficiently steep uppermost transport area (e.g., not the case for debris slide *Svidalen 4*). The attempt to quantify this impression was not conclusive due to the restricted number of shallow landslides with required estimates of initiation volume.

Source areas of the observed landslides are situated high up on hillslopes in the transition between bare bedrock and thin soil cover, commonly above or at the tree line and at the bottom of either major or minor cliffs. The vast majority of source areas received surface runoff from small- to moderately-sized uphill terrain, but since rainfall intensity high up in the mountains was even more extreme than on the lower slopes (see Fig. 2) these accounted for extraordinary amounts of water. An eyewitness has reported that spontaneous waterfalls developed along the cliff passage at Kvamsfjellet and Halvgjerda to a much greater extent than during previous storms (Sandvoll, 2020). Berti et al. (1999) presented direct field observations from a summer thunderstorm-induced debris flow in the Dolomites which is comparble in terms of the meteorological situation and with the occurrence of failure at the bottom of an ephemeral waterfall; the source area, however, is a channel bed, not on an open hillslope. This difference points to much longer return periods for summer thunderstorms of this intensity in Norway.

Whilst we observed sliding planes developed on bedrock, soft sediment and diamict, the failing material was boulder-rich diamict for all of the most far-reaching debris flows. This, together with the observation of the boulder which was transported 15 metres downhill in the starting area of debris flow *Tindefjellet 8*, points to the significance of boulders in the landslide triggering process. Small initial failures in soft sediment may mobilise boulders, which then give greater momentum to the initial mass and enable the triggering of a larger sediment volume. Another significance of boulder-rich failing material, sometimes combined with turnover of trees, is the possibility of creating blockages in gentler terrain while the water continues and intensifies its downward course, potentially triggering new debris flows in steeper downhill terrain (this was the case for for *Slåtten 1* and *2*; Fig. 8B).

Characteristics of transport areas

As suggested in the above paragraph, slumps and debris slides which did not develop into debris flows either did not have sufficient release volume or sufficiently steep slope angles in the uppermost transport area. In fact, all the large debris flows are characterised by cliff passages in their upper tansport areas with slope angles well beyond 40 degrees (i.e., at Slåtten, Vassenden and Årnes). Since the majority of source areas are high up on the hillslopes, in areas with thin soft-sediment cover, the restricted initiation volumes seem to be outweighed by the large momentum attained as the debris shoots down cliffs in the upper transport areas. For hillslope debris flows in Switzerland Hürlimann et al. (2015) found that water- and clay content have a larger influence on runout than the initial volume. For the widest debris flows and debris avalanches (in particular *Slåtten 4* and *Årnes*), erosion down to the

bedrock was restricted to the main channels in the lower transport areas. Taking the generally thick soft-sediment cover (2–10 metres) in these areas into account, it is not surprising that erosion is focused in the pre-existing channels. It is intriguing that the erosion surface over large parts of the lower transport areas at *Slåtten 4* and *Årnes* does not correspond to the transition from consolidated grey to loose brown diamict, but instead was found to be located 10–50 cm above this lithological boundary. This can be interpreted as another indication that the soil was not entirely saturated at the time of the landslide release. Given that the transition between wet topsoil and dry deeper soft-sediment cover was situated up to half a metre above the grey to brown lithological boundary, sediment entrainment was efficiently hindered by this transition from saturation to non-saturation and the erosional surface developed at this level. As a result of restricted sediment entrainment, the Jølster landslides do not seem to have reached as large volumes as comparably sized landslides elsewhere can attain. Consequently, the water-to-solid ratio was likely also higher than for shallow landslides that fail in fully saturated soils. For Årnes, the total erosion volume was calculated to 1 503 m^3, placing this debris avalanche on the lower end of observed debris flow magnitudes in relation to basin size (Marchi & D'Agostino, 2004). Taurisano (2020) used Slåtten, Jølster, as one of 11 case studies to explore whether RAMMS::DebrisFlow can produce reasonable runout paths and lengths for non-channelised shallow landslides in Norway. Taurisano's (2020) general conclusions are that the use of standard frictional parameters (ξ = 200 m/s2; μ = 0.2) and consideration of erosion in densely packed sediments (erosion rate 0.013 m/s) produces overall best results when modelling non-channelised shallow landslides. However, the Slåtten debris flows were an exception to this conclusion, since conservative frictional parameters (ξ = 3000 m/s2; μ = 0.05) and no erosion gave more realistic results (i.e., more confined flow paths and slightly shorter runouts) than the generally favoured version. The necessity to use conservative frictional parameters is consistent with the highly liquid debris flows which would be subject to very low frictional resistance. Consequently, deposits from landslides triggered during torrential summer rain, in particular after periods of drought, are expected to be more liquid, have longer runouts, but also to be slightly less destructive, given the higher water-to-solid ratio of the mobilised material.

Characteristics of landslide deposits

Another line of evidence for the restricted erosional capacity and relatively high water-to-solid ratio, was found in the deposition areas of many of the shallow landslide paths in Jølster. Landslide debris deposited in levees, in flatter sections of the landslide paths and in the final deposition areas is of restricted volume as compared with the erosional area along the flow paths. Highly water-saturated matrix was initially observed in the depositional areas of the large debris flows at Vassenden and Slåtten, but the fine to medium fraction was significantly reduced in volume after settling. This results in overall thin landslide deposits (often <10 cm) where the most promenent ingredients were wooden logs and angular boulders up to several metres in diameter, transported far along the valley bottom (Fig. 10A, C). After decades have passed, logs will have decomposed, and the thin fine- to medium-grained matrix will have been washed out, incorporated in new soil and covered by vegetation, while the angular boulders will likely be the most long-lived superficial remains of these deposits. Observations in the source areas and along the avalanche paths suggest that the boulders are partly derived from freshly weathered bedrock, remobilised till and rockfall deposits. All of these origins may result in angular to subangular boulders which, when occurring isolated at a distance from a steep cliff, are likely to be misinterpreted as rockfall deposits rather than debris flows. When conducting hazard mapping, this could lead to a misconception of which processes are dominant in the area, as natural outcrops showing the landslide sequence in sediment stratigraphy are seldom available. Boulders found in the spruce forest at Løsetslåtten are one such example. Intuitively, these would be interpreted to be the result of rockfalls, but they could also originate from rockfalls with much shorter runout which have subsequently been remobilised by one or several debris flows.

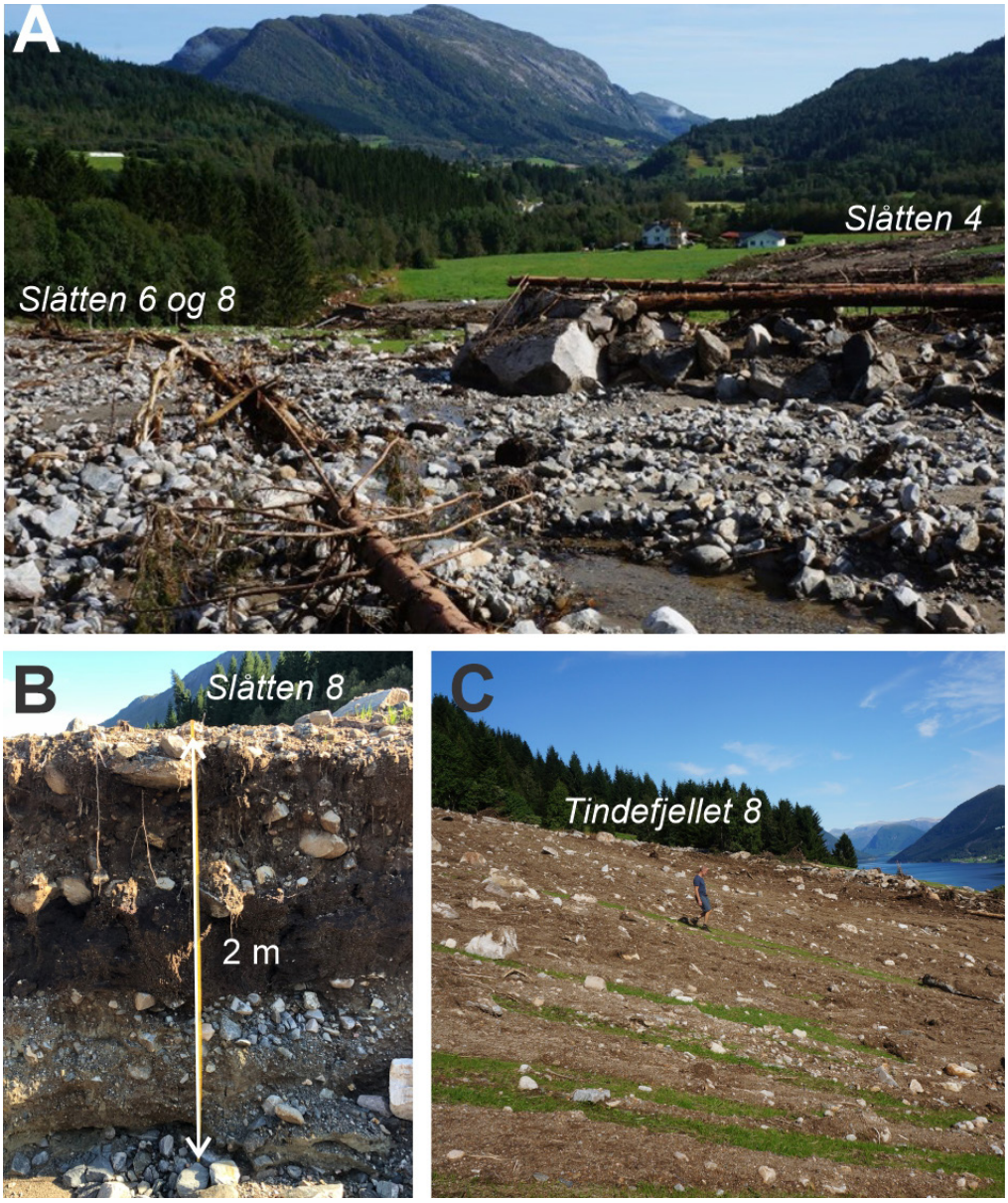

Figure 10. Examples of landslide deposits (A) Depositional area for landslides Slåtten 6 and 8 in the foreground and Slåtten 4 in the distance. (B) The stratigraphy on the farmland at Slåtten is indicative of deglacial sediments, mass movements in early Holocene followed by thousands of years with accumulation of organic material in a bog which was drained by a large debris flow event. (C) Depositional area along debris flow path Tindefjellet 8 in in open and low angle (20 degrees) farmland between 350 and 275 masl, the debris is spread out and deposited over a maximum width of 140 metres.

Supporting the above conclusions are observations at Slåtten where channel erosion across the depositional area of debris flow *Slåtten 8* revealed a 2-metres soft-sediment cover consisting of (from the bottom and upwards): 70 cm of stratified material, with well sorted silt, moderately sorted diamict and unsorted diamict with angular small cobbles, overlain by 50 cm of peat followed by 50 cm of unsorted diamict with subangular large cobbles and 30 cm of soil with occasional boulders (Fig. 10B). This stratigraphy is indicative of deglacial sediments, possibly mass movements in early Holocene time followed by thousands of years with peat accumulation in a bog which was overrun by a large debris flow event and later possibly another debris flow in more recent times, when the area was already under cultivation. Consequently, even when vertical outcrops are present, it is important to note that not every debris-flow event creates a thick layer of unsorted diamict. Summing up, intense summer rainfalls following periods of drought create spatially highly variable landslide deposits: from diamict dominated by angular boulders, over thin unsorted to layered diamict to almost isolated cobbles and boulders on an otherwise fine-grained sediment surface.

Conclusions

Based on presented weather data, detailed field observations and mapping of 52 shallow landslides, we summarise the following findings:

- Direct measurements of precipitation and weather radar data from the landslide event on 30 July 2019 in Jølster suggest exceptionally high rain intensities, exceeding the 200-year event magnitude.
- The spatial pattern of high rain intensities based on radar data is in close correspondence with observed clusters of landslides and floods. The highest rainfall intensities and greatest damage occurred in the former Jølster municipality (now Sunnfjord municipality) at the western end of lake Jølstravatnet.
- Critical precipitation values for landslide release were reached less than 2 hours after the onset of the torrential rainfall in most locations, while the last, fatal, landslide event at Årnes was preceded by less intense but longer lasting rainfall.
- Source areas of the landslides in this study are situated in the upper parts of hillslopes, at the transition between bare bedrock and thin soil cover, mostly at or above the tree line and at the foot of either major or minor cliffs.
- Open fissures in the topsoils and ground vegetation were observed in the lateral continuation of, or directly above, the backscarps at several landslide starting points.
- Based on field observations and meteorological conditions before and during the event, it is reasonable to suggest that the trigger mechanism for the Jølster shallow landslides was locally high porewater pressure due to intense rainfall and surface runoff. The runoff rapidly penetrated pre-existing openings and fissures in the rather dry soil, often at soil-bedrock or soil-boulder contacts, built up water pressure and reduced friction locally. These very local high water pressure points then formed the landslide release mechanism, rather than high general porewater pressures in fully saturated soils and peaking groundwater levels.
- Our observations of the Jølster event show anomalous behaviour of landslides triggered by heavy summer rainstorms on comparatively dry soils when compared with other seasons. These differences require revised procedures for identification of potential source areas, modelling of landslide paths and runout with higher water content, as well as the identification of landslide deposits in the field during landuse planning.
- We observed spatially very variable deposits from the largest debris flows: from thin diamict dominated deposits with angular boulders, over thin unsorted to layered diamicts, to almost isolated cobbles and boulders with little or no matrix. The last category is so far from the normally recognised landslide deposits that we postulate that after some years they are likely to be misinterpreted as the result of single rockfall events rather than shallow landslides.

Acknowledgements. Denise Rüther's contribution is funded by a start-up grant provided by the Norwegian Research Centre on Sustainable Climate Change Adaptation (NORADAPT). Bachelor students Ruben Andre Jacobsen, John Didrik Hovland Kleppe and Kjetil Skrede, as well as master student Synne Sandvoll, were supervised as part of this project and participated in fieldwork at Årnes and Slåtten, respectively. Christoffer Artturi Elo from MET has generously provided the weather radar data and technical guidance. We thank engineers at HVL, Sigurd Daniel Nerhus, and at NGI, Sean Salazar and Helge Smebye, for their contributions to the drone surveys. Jose Pullarello, NGU, is thanked for drone images from Slåtten 1. Øyvind Høydal and Frode Sandersen at NGI contributed by sharing thoughts, observations and photos from their field work in the area. Our gratitude further goes to one anonymous reviewer and Giuseppe Esposito for providing thorough and constructive feedback to the manuscript.

References

Abdella, Y., Engeland, K. & Lepioufle, J.-M. 2012: Evaluation of radar-derived precipitation estimates using runoff simulation: report for the NFR Energy Norway funded project 'Utilisation of weather radar data in atmospheric and hydrological models'.

Agersten, S., Håvelsrud Andersen, A.S., Celine Berger, A., Verpe Dyrrdal, A., Køltzow, M. & Tunheim, K. 2019: Intense byger med store konsekvenser i Sogn og Fjordane 30. Juli 2019, 41. MET-info 25–2019.

Berti, M., Genevois, R., Simoni, A. & Tecca, P.R. 1999. Field observations of a debris flow event in the Dolomites. Geomorphology 29 (3). https://doi.org/10.1016/S0169-555X(99)00018-5

Bogaard, T.A. & Greco, R. 2016: Landslide hydrology: from hydrology to pore pressure. Wiley Interdisciplinary Reviews: Water 3, pp. 439–459. https://doi.org/10.1002/wat2.1126

Bondevik, S. & Aa, A.R. 2014: Skred utløyst under uvêret Loke 14. november 2005.

Bondevik, S. & Sorteberg, A. 2021: Groundwater fluctuations during a debris flow event in Western Norway–triggered by rain and snowmelt. Hydrology and Earth System Sciences 25, pp. 4147–4158. https://doi.org/10.5194/hess-25-4147-2021

Elo, C.A. 2012: Correcting and quantifying radar data. MET-report 02-2012.

Gabet, E.J. & Mudd, S.M. 2006: The mobilization of debris flows from shallow landslides. Geomorphology 74, pp. 207–218. https://doi.org/10.1016/j.geomorph.2005.08.013

Guzzetti, F., Peruccacci, S., Rossi, M. & Stark, C.P. 2008: The rainfall intensity–duration control of shallow landslides and debris flows: an update. Landslides 5, pp. 3–17.
https://doi.org/10.1007/s10346-007-0112-1

Hanssen-Bauer, I., Drange, H., Førland, E.J., Roald, L.A., Børsheim, K.Y., Hisdal, H., Lawrence, D., Nesje, A., Sandven, S. & Sorteberg, A. 2009: Climate in Norway 2100. Background information to NOU Climate adaption., Norsk klimasenter, Oslo, Norway.

Hefre, H., Gauer, P., Høydal, Ø., Sandersen, F., Kristensen, K., Breien, H., Ekseth, K., Thygeson, K.S., Gisnås, K. & Mo, K. 2019: Faresonekartlegging i Jølster kommune.
http://publikasjoner.nve.no/eksternrapport/2019/eksternrapport2019_45.pdf

Hungr, O., Leroueil, S. & Picarelli, L. 2014: The Varnes classification of landslide types, an update. Landslides 11, pp. 167–194. https://doi.org/10.1007/s10346-013-0436-y

Høydal, Ø. & Sandersen, F. 2019: Faresonekartlegging i Jølster kommune Tileggsrapport til faresone-kartlegging i Jølster kommune - ekstern rapport 45/2019.
https://publikasjoner.nve.no/eksternrapport/2019/eksternrapport2019_69.pdf

Hürlimann, M., McArdell, B.W. & Rickli, C. 2015: Field and laboratory analysis of the runout characteristics of hillslope debris flows in Switzerland. Geomorphology 232, pp. 20–32.
https://doi.org/10.1016/j.geomorph.2014.11.030

Iverson, R.M. 1997: The physics of debris flows. Reviews of Geophysics 35, pp. 245–296. https://doi.org/10.1029/97RG00426

Iverson, R.M., Reid, M.E. & LaHusen, R.G. 1997: Debris-flow mobilization from landslides. Annual Review of Earth and Planetary Sciences 25 (1), pp. 85–138. https://doi.org/10.1146/annurev.earth.25.1.85

Jaedicke, C., Solheim, A., Blikra, L., Stalsberg, K., Sorteberg, A., Aaheim, A., Kronholm, K., Vikhamar-Schuler, D., Isaksen, K. & Sletten, K. 2008: Spatial and temporal variations of Norwegian geohazards in a changing climate, the GeoExtreme Project. Natural hazards and earth system sciences 8, pp. 893–904. https://doi.org/10.5194/nhess-8-893-2008

Johnson, K.A. & Sitar, N. 1990: Hydrologic conditions leading to debris-flow initiation. Canadian Geotechnical Journal 27, pp. 789–801. https://doi.org/10.1139/t90-092

Kalajdzic, P. & Folkman, V. 2019: Dette skjedde i Jølster. https://www.nrk.no/norge/dette-har-skjedd_tidslinje-jordras-jolstra-1.14644500, Last accessed: 31 August 2022.

Larsen, H.B. 2021: Physically Based Modelling of Shallow Landslides with "TRIGRS", Master Thesis, Norwegian University of Science and Technology (NTNU), 92pp.

Lindsay, E., Frauenfelder, R., Rüther, D., Nava, L., Rubensdotter, L., Strout, J. & Nordal, S. 2022: Multi-Temporal Satellite Image Composites in Google Earth Engine for Improved Landslide Visibility: A Case Study of a Glacial Landscape. Remote Sensing 14, 2301. https://doi.org/10.3390/rs14102301

Marchi, L. & D'Agostino, V. 2004: Estimation of debris-flow magnitude in the Eastern Italian Alps. Earth Surface Processes and Landforms 29, pp. 207–220. https://doi.org/10.1002/esp.1027

NVE. 2019: Mye regn på kort tid ga store skader i Sogn og Fjordane 30. juli 2019. https://www.varsom.no/nytt/nyheter-flom-og-jordskred/mye-regn-pa-kort-tid-ga-store-skader-i-sogn-og-fjordane-30-juli-2019/, Last accessed: 31 August 2022.

NVE. 2020: Flom- og jordskredåret 2019. https://www.varsom.no/nytt/nyheter-flom-og-jordskred/flom-og-jordskredaret-2019/, Last accessed: 31 August 2022.

Reksnes, A.H. & Grimeland, P.K. 2019: Politiet opna vegen der bil vart teken av ras – no beklagar dei. https://www.nrk.no/vestland/politiet-opna-vegen-for-raset-kom-1.14645394, Last accessed: 31 August 2022.

Sandvoll, S. 2020: Romleg og temporal fordeling av styrtregnet og skredhendingane i Jølster 30. juli 2019, Master Thesis, Western Norway University of Applied Sciences (HVL).

Sandersen, F., Bakkehøi, S., Hestnes, E. & Lied, K. 1997: The influence of meteorological factors on the initiation of debris flows, rockfalls, rockslides and rockmass stability. In Senneset, K. (ed): Landslides. Proceedings of the 7th Symposium on Landslides, pp. 97–114.

Schilirò, L., Cepeda, J., Devoli, G. & Piciullo, L. 2021: Regional Analyses of Rainfall-Induced Landslide Initiation in Upper Gudbrandsdalen (South-Eastern Norway) Using TRIGRS Model. Geosciences 11, 35 pp. https://doi.org/10.3390/geosciences11010035

SeNorge. 2022: Precipitation Reference period. https://senorge.no/map, Last accessed: 31 August 2022

Taurisano, A. 2020: FOU 80607 - RAMMS::Debris Flow for beregning av jordskred – Casestudier og anbefalinger for bruk. https://publikasjoner.nve.no/eksternrapport/2020/eksternrapport2020_20.pdf

Tichavský, R., Ballesteros-Cánovas, J.A., Šilhán, K., Tolasz, R. & Stoffel, M. 2019: Dry spells and extreme precipitation are the main trigger of landslides in Central Europe. Scientific Reports 9, pp. 1–10. https://doi.org/10.1038/s41598-019-51148-2

Varnes, D.J. 1978: Slope movement types and processes. Special report 176, pp. 11–33.

xGeo. 2019a: Degree of soil saturation 30 July 2019 8 am. http://www.xgeo.no, Last accessed: 31 August 2022.

xGeo. 2019b: Ground water level compared to normal 30 July 2019 8 am. https://www.xgeo.no, Last accessed: 31 August 2022.

Ødemark, K., Førland, E., Mamen, J., Elo, C.A., Dyrrdal, A.V. & Myrabø, S. 2012: Ekstrem korttidsnedbør på Østlandet fra pluviometer og radar data. http://hdl.handle.net/11250/2497281